Microstructured Optical Fibers filled with Carbon Nanotubes: Photonic Bandgap Modification and Sensing Applications

Marco Pisco[1], Marco Consales[1], Antonello Cutolo[1], Patrizia Aversa[2], Michele Penza[2], Michele Giordano[3] and Andrea Cusano[1]
[1]*University of Sannio, Optoelectronic Division, Engineering Department, Benevento, Italy*
[2]*ENEA, C.R. Brindisi, Materials and New Technologies Unit, Brindisi, Italy*
[3]*National Research Council, Institute for Composite and Biomedical Materials, Napoli, Italy*

1. Introduction

In the recent years, a new concept is emerging in the scientific community dealing with the possibility to use optical fibers as platform to develop all-in-fiber multimaterial and multifunctional optical devices and systems (Abouraddy et al., 2007). The key feature of these new optoelectronic devices relies on the proper integration of specific materials, such as conductors, semiconductor and insulator, into the same optical fiber in order to attain advanced functionalities within a single optical fiber. A promising building block to realize these multifunctional optoelectronic devices are the Microstructured Optical Fibers (MOFs) which, being composed by a periodic distribution of micrometric air-holes running uniformly along the fiber length (Knight et al., 2003), offer an high degree of freedom in their fabrication and at the same time several opportunities of integration with specific materials. Also by manipulating the properties of the in-fiber integrated materials, the guiding features of the MOF itself can be properly changed in order to develop new tunable photonic devices (Domachuk et al. 2004; Larsen et al. 2003; Huang et al. 2004) as well as optical fiber sensors (Benabid et al. 2005; Matejec et al. 2006).
Single Walled Carbon Nanotubes (SWCNTs) constitute a very promising material for multimaterial and multifunctional photonic devices in light of their unique electrical and mechanical properties (Dresselhaus et al. 2001). Furthermore, the opto-chemical sensing properties of carbon nanotubes, deposited onto singlemode standard optical fiber (SOF) configured in buffered and not buffered reflectometric configurations, have been demonstrated to be suitable (Penza et al. 2004; Penza et al. 2005 ; Consales et al. 2006; Consales et al. 2007) to perform chemical detection of volatile organic compounds (VOCs) at room temperature.

This chapter reviews the research activities devoted to the integration of MOFs with Single Walled Carbon Nanotubes (SWCNTs) for the realization of new all-in-fiber active and passive photonic devices (Cusano et al. 2006; Pisco 2007; Pisco et al. 2008; Pisco et al. 2009).
The chapter starts with the description of the procedure to fill the MOFs with SWCNTs by Langmuir-Blodgett (LB) technique. The attention is then focused on the individuation of the main trends and correlations between the deposition process parameters and the MOF guiding properties modifications due to the SWCNTs integration. To this aim, both morphological characterizations and far field transmission measurements were performed. The activities about the integration between MOF and SWCNTs have been hence finalized and exploited for VOCs detection applications. In this framework, the sensing probes, fabricated with different process features, have been characterized by reflectance spectra measurements in order to get more information on the nanotubes filling within MOF holes. The realized sensors, employed in single wavelength reflectometric configuration, have been then exposed in a test chamber to several VOCs pulses at room temperature in order to demonstrate their capability to work for sensing applications.
The experimental results here reported demonstrate the success of the SWCNTs infiltration within the HOF holes and the capability to modify the guiding properties of HOFs by acting on deposition process features. Furthermore, the experimental measurements performed in a test chamber reveal that MOFs-SWCNTs sensing probes can be exploited to realize novel opto-chemical sensors for VOCs detection with a good sensitivity and fast response times.

2. Methodology

Several samples have been arranged by injecting SWCNTs within the MOF holes and the MOF Photonic Band-Gap (PBG) features dependence on the deposition parameters has been investigated by far field transmission measurements. The samples were composed by a piece of MOF, spliced at one end with a SOF and covered and partially filled with SWCNTs at the other termination as schematically shown in the figure 1. Before the MOF-SOF splicing, the deposition of SWCNTs was performed at atmospheric pressure by means of the LB technique described in the following.

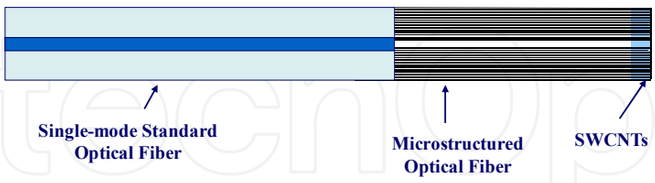

Fig. 1. Schematic view of the MOF-SWCNTs samples

2.1 The Langmuir-Blodgett Technique

The LB technique allows to deposit defect-free and molecularly ordered ultra-thin organic films of SWCNTs pristine material onto a substrate (Penza et al. 2005). This deposition technique has been yet widely used to transfer SWCNTs onto planar substrates as well as onto SOF ends (Penza et al. 2004; Penza et al. 2005) and it is here employed to integrate carbon nanotubes within the holes of MOFs. With this technique, the molecules of the films to be deposited are firstly dispersed onto the surface of a sub-phase, typically oriented with

the hydrophobic part upwards and with the hydrophilic one immersed in water. Subsequently, a reduction of the surface area occupied by each molecule is performed by means of moving barriers in order to produce a solid phase of a given surface pressure in which the molecules are densely packed forming a highly ordered array. From this phase the molecules can be transferred to a properly cleaned and prepared solid substrate by its dipping through the condensed Langmuir layer.
Since the solid phase is reached only at a proper surface pressures, a continuous reduction of the moving barriers is performed when the molecules are transferred from the sub-phase to the substrate in order to keep the surface pressure constant, ensuring that the solid phase is maintained. Repeated dipping of the same substrates results in an accurate nano-sized monolayer by monolayer deposition.
In particular, for the integration within MOFs, a solution (0.2 mg/ml) of SWCNTs pristine material (purchased from Carbon Nanotechnologies Inc., Houston, USA) in chloroform has been spread onto a sub-phase constituted by deionised water (18 MΩ) with 10-4 M of $CdCl_2$. The sub-phase pH and the temperature were 6.0 and 23°C, respectively. The monolayer has been compressed with a barrier rate of 15 mm/min until the surface pressure of 45 mN/m is reached. The single layer has been deposited with a dipping rate of 3 mm/min and the transfer ratio of the monolayer from the sub-phase to the substrate surface was in the range 0.5 to 0.7.
Although the LB deposition method is a well-assessed technique, the employment of the LB technique to integrate carbon nanotubes monolayers within the MOF holes yields substantial changes in the deposition process.

Sample	Length (cm)	Monolayer
1	13.3	10
2	11.0	16
3	4.0	20
4	10.0	20
5*	6.5	20

Table 1. Samples main features (* SWCNTs deposited after the SOF-MOF splicing)

As matter of fact, the microstructuration of the substrate, constituted by the MOF, affects the deposition process in light of the micrometric dimensions of the MOF holes enabling capillarity phenomena (Nielsen et al. 2005; Zhmud et al. 2000). During the vertical MOF dipping, performed with the rate of 3 mm/min and for a depth of 1mm, it is expected that the LB suspension penetrates within the MOF holes for effect of the dipping itself and at the same time rises within the MOF holes for capillarity. It is worth to highlight that the penetration depth of the LB suspension within the MOF holes does not correspond to the penetration depth of the SWCNTs within the MOF holes. The SWCNTs deposition occurs with an high efficiency at a given suspension surface pressure while the dipping of the MOF

substrate, breaking the superficial regularity of the suspension, locally changes the parameters ruling the effectiveness of the carbon nanotubes deposition on the microstructured substrate. Furthermore, the extension of the region onto the holes sides where the nanotubes adhered is limited from the quantity of carbon nanotubes "available" at the dipping time. Differently from the classic LB deposition on a planar substrate accomplished with a constant surface pressure, here, even if the overall surface pressure is held constant by the barrier movement, locally at each MOF hole, only the nanotubes sub-phase corresponding to the MOF hole affects the deposition during the dipping. In summary it is expected that the transfer of SWCNTs thin monolayers within the MOF holes by means of the LB deposition method would be the result of the dipping movement and capillarity's phenomena rising at the dipping time strongly dependent on the surface pressure. It is noteworthy that while the capillarity phenomena impose differences in the carbon nanotubes penetration depth between the core and cladding holes due to the different diameters, the dipping movement into the suspension reduces the differences, forcing the suspension penetration at the dipping time. Nevertheless, while the adhesion and penetration mechanisms are currently under investigation, the experimental results revealing the capability to deposit SWCNTs within the MOF holes and to consequently modify the MOF guiding properties are here presented.

2.2 Splicing procedure between MOF and SOF

The open end of the MOF piece has been spliced at the input end to a SOF by using an electrical arc splicing system (Fujikura FSM-50S). The fibers ends, both cleaved, have been aligned and pressed against each other using the splicer precision motors. In order to avoid the collapse of air holes during the splicing, a splicing procedure has been developed ad hoc. In particular, a series of ten arcs with short duration (100ms) and high power (80bit power) have been forced, in place of a single arc with lower power (40bit) and longer extension (800ms) usually used for SOF-SOF splicing. The splicing process was previously tested and the losses were estimated to be about 1dB by means of the comparison between the measurements of the transmitted power in butt coupling configuration and after the optical fibers fusion respectively. In addition, the bonding achieved between the two fibers, weak with respect to the bending, has been enforced by using an heating protection sleeve.

3. Experimental

The SWCNTs monolayers deposition has been accomplished on several pieces of MOF with different length on the order of few centimeters and it was performed at atmospheric pressure with the other MOF termination not connected. After the deposition, for each sample, the free termination has been then spliced at a single-mode SOF. Several samples have been realized with the LB technique by changing the monolayer number and thus the amount of carbon nanotubes able to fill the MOF holes. In the following, the analysis is focused on five samples fabricated according to the table 1. Also the influence of the external pressure at the dipping time has been investigated by depositing 20 monolayers of SWCNTs onto an MOF piece previously spliced to a SOF (sample 5).

3.1 Morphological characterization

In order to investigate the morphological characteristic of the fabricated MOF samples, a Scanning Electron Microscope (SEM) has been used. The analysis with the SEM has been performed on several samples. The retrieved images of the observed samples show a quite uniform overlay covering the fibers holes. In fig. 2 (a-b) an Atomic Force Microscope (AFM) image of a MOF before the deposition and the SEM image of the same MOF after the deposition of 10 monolayer of SWCNTs have been reported demonstrating the success of the SWCNTs deposition onto the MOFs. In figure 2 (c-d), instead, the SEM image of a bare MOF and the SEM image of the MOF after the deposition of 16 monolayer of SWCNTs (sample 2) have been reported. The SEM images, showing a particular of the MOF cladding, reveal a web-like overlay covering the MOF holes demonstrating the success of the SWCNTs deposition onto the MOFs.

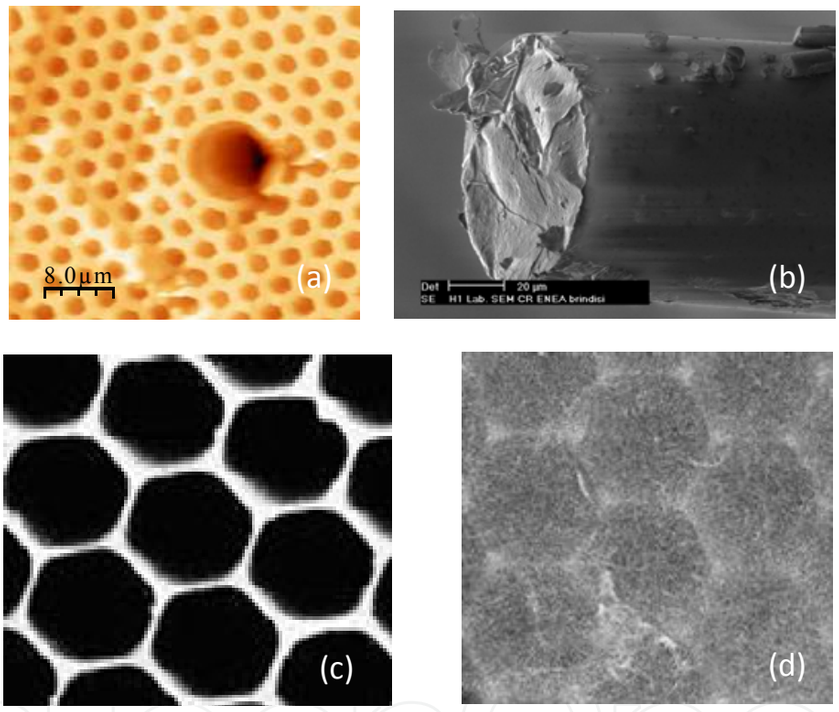

Fig. 2. AFM image of a bare MOF (a), SEM image of the MOF after the deposition of 10 monolayer of SWCNTs (b), SEM image of a bare MOF (c) and SEM image of the MOF after the deposition of 16 monolayer of SWCNTs (d). (Fig. 2 (c-d): Reprinted with permission from ref. (Pisco et al. 2009))

3.2 Far field Characterization and Bandgap Modification

In order to characterize the MOF-SWCNTs guiding properties modifications and the SWCNTs filling capability, the optical far field emerging from the samples has been collected by means of an infrared vidicon camera (Hamamatsu C2741-03) while a narrowband laser source at 1550nm lights the samples. The camera has been screen-shielded from the visible light and a proper holder for the fiber has been provided in order to guarantee the repeatability in the positioning of different samples. In figure 3 is schematically reported the experimental setup employed for the far field characterization.

The end face of the samples has been positioned in the nearby of the receiving lens. In figure 4 (a) the transmission field, revealed in far field mode, of an MOF without nanotubes is reported as reference. The far field emerging from an MOF is characterized, as known (Knight et al. 2003), by a Gaussian shape due to the MOF fundamental mode except for the presence of little peaks of circular shape corresponding to the cladding holes close to the core.
In the figure 4 (b) and 4 (c) the emerging far fields from the samples 1 and 2 realized with 10 and 16 monolayers are reported, respectively. As observable, the presence of the SWCNTs is not able to strongly modify the field distribution of the propagating mode which basically keeps the Gaussian shape. Nevertheless, while for the sample 1, a slightly higher light content can be observed in correspondence of the MOF cladding in the coated case, the same spreading of the far field is more evident for the sample 2 which exhibits a stronger increase of the field amplitude external to the corresponding fiber core.

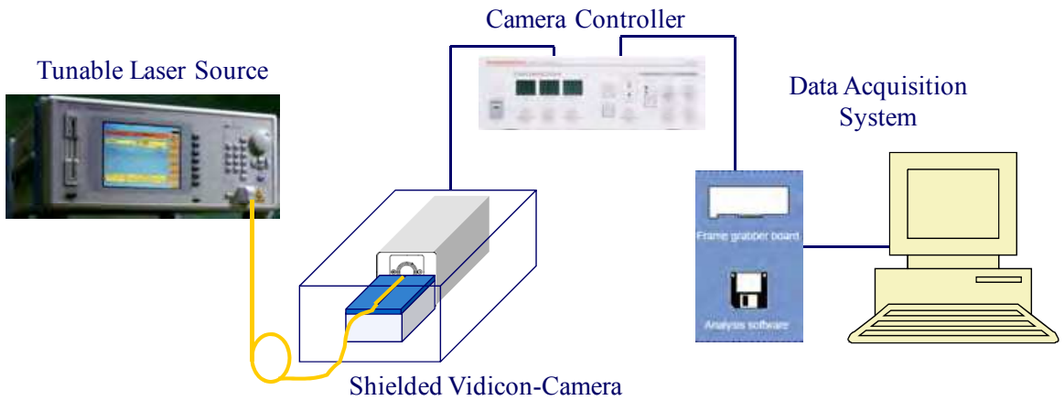

Fig. 3. Experimental setup for the Far Field characterization

The far field spreading increases with the monolayer number and thus accordingly to the higher SWCNTs content. As evident, the main effect of SWCNTs filling is a worse confinement of the fundamental mode, consistent with a refractive index contrast reduction induced by a partial filling of the core and cladding holes. It is noteworthy that the core refractive index increase (with no cladding holes filled) is expected to lead to an increase of the core confinement power, while the cladding holes refractive index increase (with core unperturbed) as well as the core and cladding holes refractive indexes simultaneous increase would lead to a diminution of the fundamental mode confinement power. Hence the field spreading observed between the samples with 10 and 16 monolayer and the bare MOF is in agreement with an increase of the cladding holes refractive index or of the core and cladding holes refractive indices. Nevertheless the exclusive cladding holes filling is not expected on the basis of the deposition technique used except for differences in the carbon nanotubes penetration between the core and cladding holes due to the different capillary diameters. With regard to the sample 3, a strong modification of the field distribution occurs and the amount of power transmitted is strongly reduced as reported in figure 4 (d). The emerging field presents a circular crown shape and the core mode is not more visible. In other words, the larger amount of SWCNTs used for sample 3 is able to induce a strong diminution of the fundamental mode power, attributable to the modification of the PBG occurring in consequence of the MOF holes filling.

Hence, the far field emerging from the sample 3, in agreement with the field exhibited from the samples 1 and 2, demonstrates the capability of the LB technique to infiltrate SWCNTs within the MOF holes. In particular, the deposition of 20 monolayers (or more) yields the functionalized MOF not more able to guide meaningfully the light. As matter of fact, the PBG modification affects particularly the field distribution of the sample 3 which was fabricated with an higher number of monolayers with respect to the samples 1 and 2.

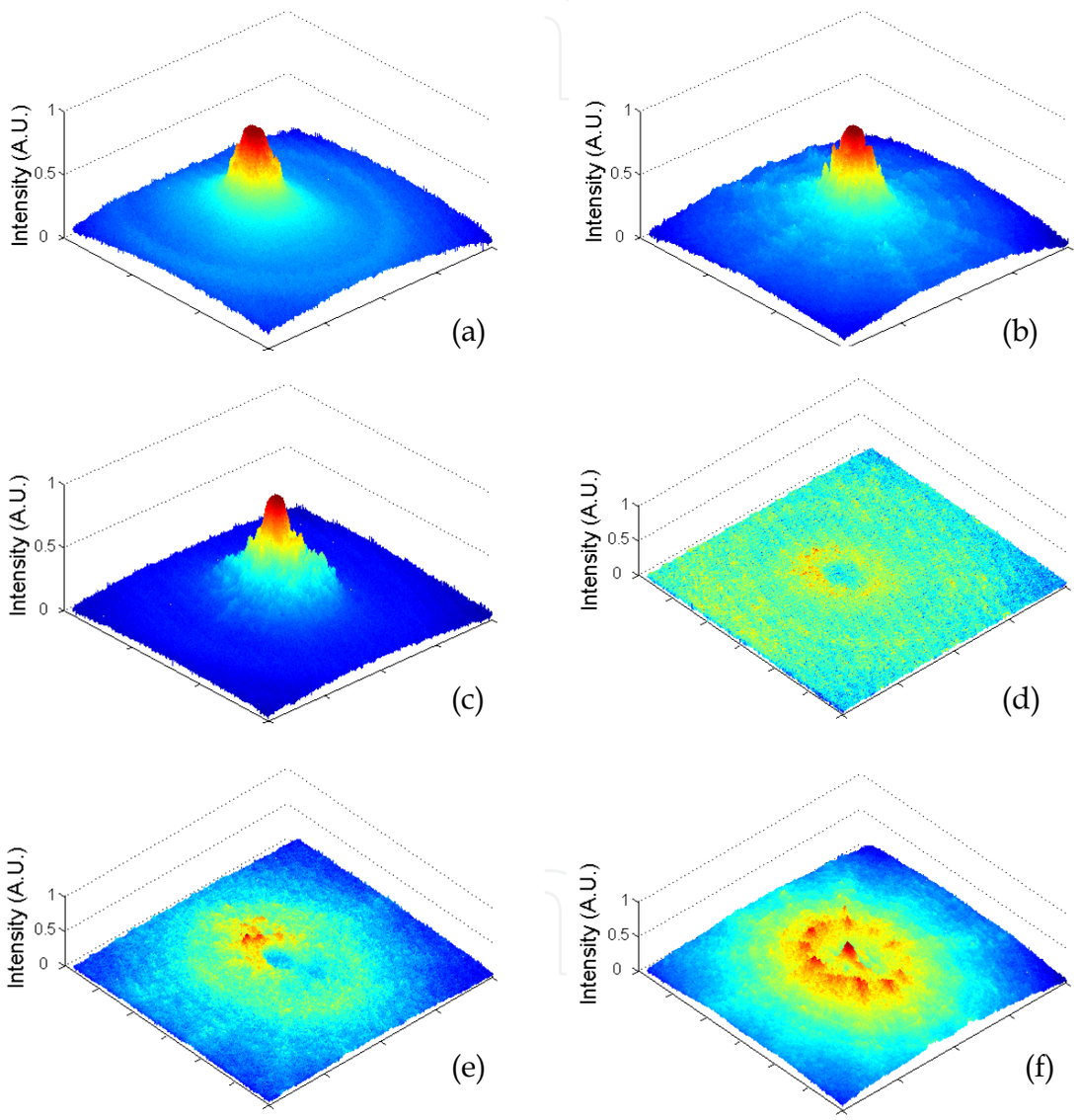

Fig. 4. Distribution of the far field of the bare MOF (a) and of the MOF samples 1-5 (b-f) respectively. (Reprinted with permission from ref. (Pisco et al. 2009))

In order to study the influence of the MOF length, the far field emerging from the sample 4 has been characterized and reported in figure 4 (e). Both samples 3 and 4 have been obtained

by depositing 20 SWCNTs monolayers, but the MOF pieces are long 4 and 10cm respectively. It is observable that the far field keeps the circular crown shape and the fundamental core mode has been suppressed again. The field emerging from the sample 4, however, is slightly circularly asymmetric and the light content is slightly higher. The comparison thus reveals that the MOF length doesn't rule meaningfully the field distribution in transmission. In addition, it confirms the important role of monolayers number in the PBG modification and thus on the resulting field distribution. It is noteworthy that this result is consistent with the deposition process previously described. In fact, assuming the deposition as the resultant of dipping and capillarity mechanisms it was not expected any dependence on the fiber length. Congruently the SWCNTs deposition is strongly affected by the number of dipping and not by the capillaries lengths.
Finally, figure 4 (f) reports the far field emerging from an additional sample on which 20 monolayer of SWCNTs have been deposited after the splicing procedure. The connection at the fiber termination is responsible for a change in the air pressure within the MOF holes and thus a less efficient filling is expected. As observable, the far field emerging from the sample presents still a circular crown shape and a little peak in correspondence of the MOF core is visible. The deposition of 20 monolayer is able to strongly modify the PBG but the core mode is not completely suppressed. In this case, during the deposition stage, the LB suspension, in order to penetrate within the MOF capillaries, had to overcome the pressure offered by the air present within the MOF. The elasticity of the air thus determines a pressure variable during the MOF dipping and it represents a good exemplification of the effect of the pressure on the deposition which can be otherwise properly controlled.
In summary, the far field characterizations reveal the success of the SWCNTs deposition demonstrating the partial filling of the nanotubes within MOFs. Also, the obtained results demonstrate that the main effect of SWCNTs filling is the significant modification of the guiding properties and thus of the local PBG at the termination of the MOF. Also, by using the LB deposition method, we demonstrate how by acting on the process parameters and especially on monolayers number and pressure conditioning at the free termination, it would be possible to optimize and tailor the SWCNTs filling enabling the local control of the MOF PBG. The proper modification of the MOF PBG features, by filling (also selectively) the MOF holes with SWCNTs, can supply, in fact, to the final device advanced functionalities and can be properly exploited to develop high performances sensors based on PBG modification as well as multimaterial and multifunctional fibers.

4. Sensing Application

In this section, we report on the exploitation of the experimental results previously described about the integration between MOFs and SWCNTs in order to develop an all fiber opto-chemical sensor useful for VOCs detection.
In the recent years, the sensing properties of carbon nanotubes deposited onto singlemode SOF configured in reflectometric configurations have been widely investigated (Penza et al. 2004; Penza et al. 2005) demonstrating their capability to perform chemical detection of VOCs at room temperature.
On the basis of the previously provided demonstration about the change of the guiding properties of the MOFs due to the presence of the sensitive materials within the MOF holes, the exploitation of the integration of MOFs and SWCNTs has been successfully employed

for the development of new in-fiber opto-chemical sensors (Cusano et al. 2006; Pisco et al. 2008) and the retrieved experimental results are here summarized.
In particular, an extensive analysis of the samples 1 and 3, employed for sensing application, is reported. It is worth remembering that the former one, labelled sensor 1, is constituted by a 13.3 cm long MOF with 10 monolayer of SWCNTs, the latter, labelled sensor 3, by a 4cm long MOF and 20 SWCNTs monolayer. Furthermore, the sensors have been characterized by reflectance spectra in order to get more information on the nanotubes filling within MOF holes. Finally the aforementioned sensors, employed in single wavelength reflectometric configuration, have been exposed in a test chamber to several toluene pulses at room temperature in order to demonstrate their capability to work for sensing applications. The experimental results obtained in this framework are presented in the following and the impact of the fabrication stage on the sensing performances is also discussed.

4.1 Reflectance Characterization

Reflectance characterization of the realized probes has been carried out within the MOF bandwidth. To the aim, by means of the experimental setup sketched in figure 5, a tunable laser source and an optical spectrum analyzer have been used in synchronous mode allowing 1pm wavelength resolution in the spectral range 1520-1620nm. In figures 6 and 7, the reflected spectra are reported for the two samples. Reflectance spectra reveal several interference fringes and also their envelope offers a quite periodic behavior. In particular, in the reflectance of the sensor 1, two different harmonic contents, fast and slow, can be clearly distinguished. The observation of two different harmonic contents suggests the presence of a double cavity interferometer. From the wavelength separation of the fringes the optical path length weighted by the medium effective refractive index of each interferometer can be approximately retrieved, according to:

$$2 \cdot n_{eq} \cdot d = \frac{\lambda_1 \cdot \lambda_2}{(\lambda_2 - \lambda_1)} \tag{1}$$

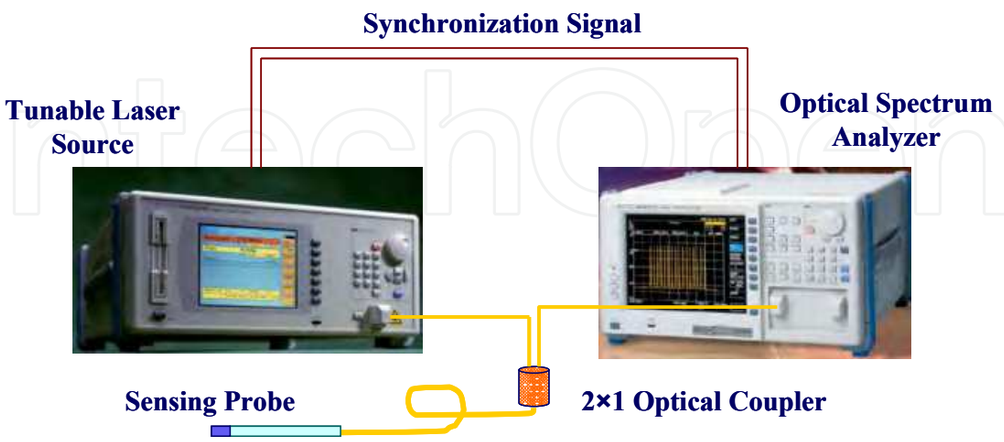

Fig. 5. Experimental setup for the spectral characterizations

where d is the length of the interferometer, n_{eq} is the medium effective refractive index of the propagating mode, λ_1 and λ_2 are the wavelengths corresponding to two adjacent

maxima. Thus, by applying twice the eq. (1) at the reflectance spectrum, the features of the double interferometer, in both fast and slow regime, can be deduced. The optical path lengths weighted by the medium effective refractive index obtained for the sensor 1 are approx. 26.6cm and 40μm respectively.

The former one coincides approximately with the double length of the MOF piece, by considering the MOF effective refractive index equal to one (not filled by SWCNTs). The latter one represents the extension of the region, on micrometric scale, constituted by the deposited SWCNTs, either they are within the MOF holes or outside of the MOF end face.

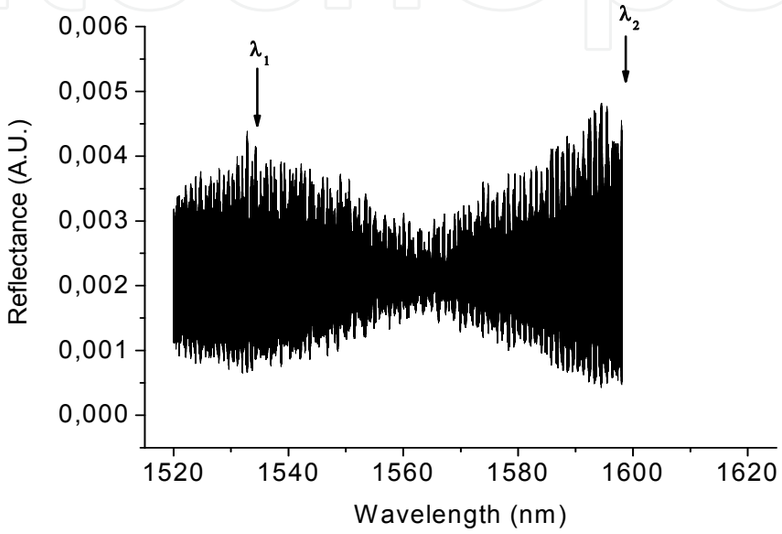

Fig. 6. Reflectance of the MOF sensor 1. The arrows indicate the wavelengths corresponding to two adjacent envelope relative maxima. (Reprinted with permission from ref. (Pisco et al. 2008))

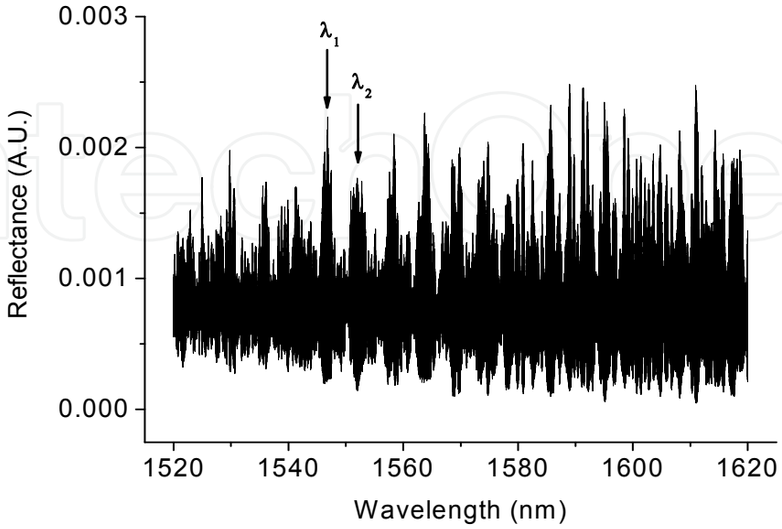

Fig. 7. Reflectance of the MOF sensor 3. The arrows indicate the wavelengths corresponding to two adjacent envelope relative maxima. (Reprinted with permission from ref. (Pisco et al. 2008))

The two cavities, hence, can be attributed to the piece of MOF and to the SWCNTs region. In turn, from the analysis of the reflectance of the sensor 3, although it is again clearly observable the fast oscillating component, the envelope of the reflectance seems to be periodic mostly in the wavelength range 1545-1575nm while it is less recognizable a periodic behavior for the envelope in the remaining spectral range.
Nevertheless, by applying also in this case twice the eq. (1), optical path lengths weighted by the medium effective refractive index of 8cm and 460μm are obtained for sensor 3. The fast oscillating behavior is still attributed to the piece of MOF, which is 4cm long, whereas the SWCNTs seem to cover a region of hundreds of microns consistently with the larger amount of SWCNTs deposited in the case of the sensor 3 (20 monolayers). Also, on the basis of previous works (Penza et al. 2005) dealing with the SWCNTs deposition onto the end face of SOFs, it results that 10 and 20monolayers of SWCNTs are not able to produce an external cavity able to produce interference fringes in the investigated wavelength range. Hence, the results obtained from the spectral characterization of both sensors reveal that the carbon nanotubes are penetrated at least in the MOF central hole and their distribution along the MOF axis, which cannot be assumed spatially uniform, extends for tens and hundred microns, respectively.
It is noteworthy that the eq. (1) is rigorously valid under the hypothesis of transparent media which in turn is not truly verified for carbon nanotubes based materials. In addition, the estimation of the equivalent cavity length by means of the interference fringes together with the trivial measurement of the length of the MOF piece before the deposition are not able to discriminate the fraction of nanotubes penetrated inside the holes from the fraction of nanotubes which composes an external overlay at MOF termination (Cusano et al. 2006). Nevertheless, an insight of the double interferometer behavior of the sensing probe is obtained and an approximated estimation of the extension of the SWCNTs region can be retrieved.

4.2 Sensor Modeling

On the basis of reflectance and far field characterizations the sensing probe reflectance of the sensor 1 can be modeled as a Fabry Perot double interferometer while the behavior of the sensor 3 cannot be trivially assumed like a simple double interferometer in agreement with the spectral and far field analysis. In eq. (2) the model of the reflectance of the sensor 1 is reported. The symbols r, n, d and A represent respectively the reflection coefficient, the complex effective refractive index, the cavity length and the absorbance (due to the coupling and splicing losses), while the subscript indices indicate the interface to which are referred as well as the subscript labels indicate the referred cavity. In particular the subscript 12 is referred to the SOF-MOF interface, 23 to the MOF-SWCNTs interface and 34 to the SWCNTs-external medium interface, while the subscript labels SOF, MOF and SWCNTs have obvious meaning. The reflectance R is ruled by several factors involved in the propagation of the lightwave through the MOF and the MOF filled with SWCNTs. In particular, any change in the SWCNTs dielectric function affects the reflectance R through the reflection coefficients r_{23} and r_{34}, the absorbance A_{23} and the propagation constant β_{SWCNTs} according to the eq. (2- 3)

$$R = \left| \frac{r_{12} + r_{23} \cdot (1 - A_{12}) \cdot e^{j \cdot \beta_{MOF}} + r_{34} \cdot (1 - A_{12}) \cdot (1 - A_{23}) \cdot e^{j \cdot (\beta_{MOF} + \beta_{SWCNTs})} + r_{12} \cdot r_{23} \cdot r_{34} \cdot e^{j \cdot \beta_{SWCNTs}}}{1 + r_{12} \cdot r_{23} \cdot e^{j \cdot \beta_{MOF}} + r_{12} \cdot r_{34} \cdot (1 - A_{23}) \cdot e^{j \cdot (\beta_{MOF} + \beta_{SWCNTs})} + r_{23} \cdot r_{34} \cdot e^{j \cdot \beta_{SWCNTs}}} \right|^2 \quad (2)$$

with

$$r_{12} = \frac{n_{SOF} - n_{MOF}}{n_{SOF} + n_{MOF}} \; ; \; r_{23} = \frac{n_{MOF} - n_{SWCNTs}}{n_{MOF} + n_{SWCNTs}} \; ; \; r_{34} = \frac{n_{SWCNTs} - n_{ext}}{n_{SWCNTs} + n_{ext}} \; ;$$
$$\beta_{MOF} = \left(\frac{4 \cdot \pi}{\lambda} \right) \cdot n_{MOF} \cdot d_{MOF} \; ; \quad \beta_{SWCNTs} = \left(\frac{4 \cdot \pi}{\lambda} \right) \cdot n_{SWCNTs} \cdot d_{SWCNTs} \quad (3)$$

It is noteworthy that the sensor sensitivity to chemical induced changes in the dielectric properties of the sensitive material used to functionalize MOFs cannot be thought as derived by a simple Fabry-Perot effect in light of the PBG modifications. For instance, at the interface between the MOF and the MOF filled with SWCNTs, coupling losses due to the modal overlap between modes propagating in the sections with different guiding properties affect the reflectance R. This means that as the dielectric function of the SWCNTs is modified by chemical sorption, consequent changes are expected in the coupling coefficients as well as in the reflectance R. On the other hand, also the propagation losses within the MOF region filled with SWCNTs depend on the SWCNTs dielectric function and hence contribute to the reflectance variations. In summary, the SWCNTs effective dielectric function variations within the MOF filled with SWCNTs determine, in combination with the penetration depth of the carbon nanotubes, the sensing probe reflectance changes by affecting the propagation features of the sensing probe itself. According to the author, the key factor in the determination of the performances of this class of sensors relies in the possibility to exploit the aforementioned losses variability in order to get enhanced performances with respect to traditional SOF-SWCNTs based sensors.

4.3 Experimental Results

In order to investigate the sensing capability of the fabricated MOF sensors, they have been placed in a test chamber (Consales et al. 2006; Consales et al. 2007) and exposed to traces of VOCs. At the same time, a reflectometric system, schematically reported in figure 8, which allows reflectance measurements at single wavelength, has been employed. In order to light the sensing probes a Superluminescent Light Emitting Diode with 40nm bandwidth centered at 1550nm has been used. By means of an optical coupler the light source is split. One of the arms of the coupler is connected directly to a photodiode in order to provide a monitoring of the source power level and the other arm is connected to the sensing probes by means of an optical switch which is responsible for the time division multiplexing allowing the simultaneous interrogation of several sensors. The time-multiplexed reflected signal is collected by another photodiode. The electrical signals coming from the photodetectors are acquired by a Data Acquisition (DAQ) system and stored in a computer which provide to the time demultiplexing of the retrieved signals. The optoelectronic sensor output consists in the ratio between the reflected signal at the sensing interface and the source reference signal.
It is worth noting that since the light source used offers a bandwidth much wider than the separation of the faster interference fringes, the sensing performance exploited by each

sensor basically depends on the slow features of the reflectance spectrum and thus mainly on the SWCNTs cavity. During the measurements, the temperature within the chamber has been monitored by using a commercial thermocouple. The sensors sensitivity to temperature variations was previously characterized and used in order to properly compensate the sensors output.

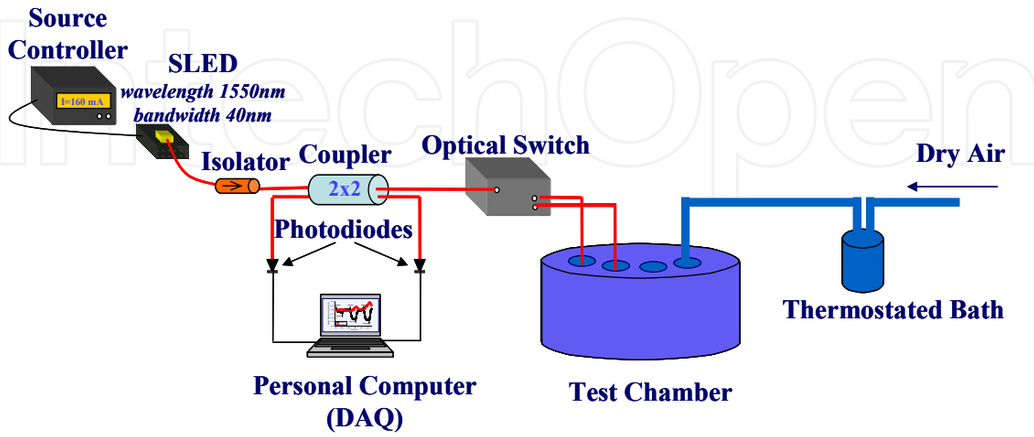

Fig. 8. Experimental setup for volatile organic compounds exposure

The optical sensors have been located in a test chamber for toluene traces exposure measurements. Dry air has been used as reference gas and carrier gas to transport the VOCs of toluene with different concentration pulses. The test cell containing the sensor had a volume of 1200ml whereas the total flow rate for each exposure has been kept constant at 1000 ml/min. The gas flow rate has been controlled by a mass flow-meter driven by a controller-unit. The VOCs vapors have been generated by the bubbling method with a thermo-stated flask containing the liquid analyte

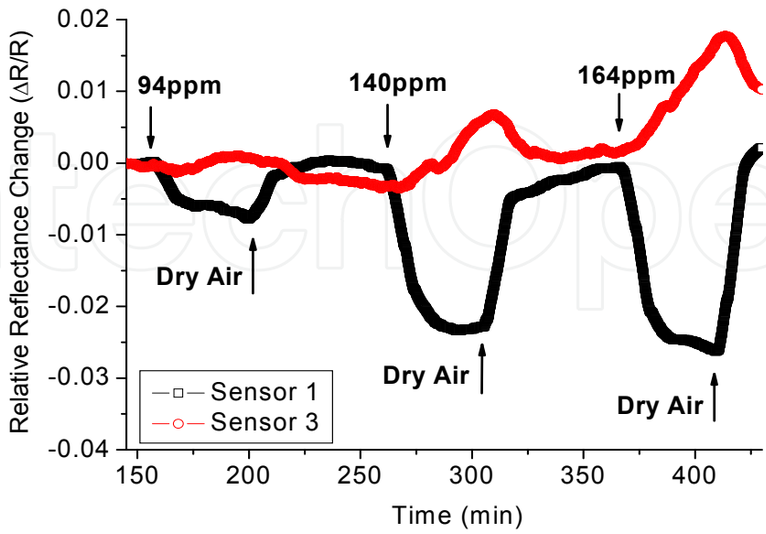

Fig. 9. Time responses of MOF sensors 1 and 3 to three toluene impulses (Reprinted with permission from ref. (Pisco et al. 2008))

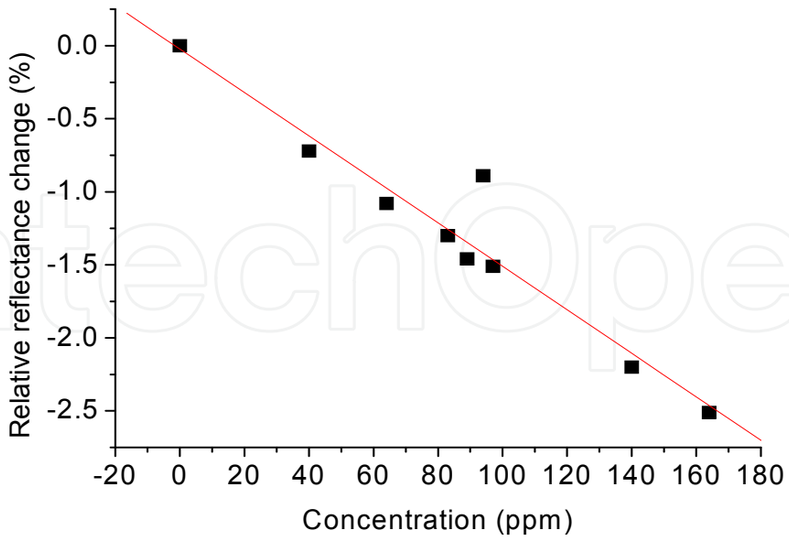

Fig. 10. Relative Reflectance Change (ΔR/R) of the sensor 1 corresponding to the steady states reached upon exposures to different concentration pulses of toluene (Reprinted with permission from ref. (Pisco et al. 2008))

Here a comparison among the performances exploited by sensors 1 and 3 is carried out by considering their relative reflectance change due to toluene exposure. To this aim, both sensors have been exposed to three toluene pulses of 45 minutes with increasing concentrations in the ppm range. Fig. 9 reports the time responses of both sensors. Upon exposures, the reflectance of the sensor 1 decreases linearly with the toluene concentration as confirmed by further exposure measurements resumed in fig. 10. Differently, sensor 3 reflectance increases upon exposure presenting a significantly lower sensitivity, opposite in sign. Moreover, sensor 3 is not able to reach a steady state within 45 minutes especially for high concentration exposures, this also limits the maximum reflectance change observed during the exposure tests. The higher response times and the lower sensitivity of the sensor 3 can be explained on the basis of the higher extension of the SWCNTs region (higher diffusion times and higher losses in the filled region). In fact, the VOCs, able to interact with the SWCNTs, lead to a change of the SWCNTs agglomerate dielectric function and the induced variations are detected as fast as short is the SWCNTs region. In addition, as demonstrated by the far field characterization, the SWCNTs penetration depth in the sensor 3 yields the functionalized MOF not more able to guide the light and thus it reduces the capability of the light to interact with the sensitive material. Further investigation is required to assess the sensitivity dependence on the SWCNTs distribution within the MOF structure and also to identify characterization features able to predict the correct functioning and the performance of the final device.

7. Conclusion

In conclusion, the research activities devoted to the integration of MOFs with SWCNTs in order to develop new in-fiber active and passive optoelectronic devices are reviewed. The infiltration of SWCNTs inside the MOF holes has been accomplished through the deposition of multiple SWCNTs monolayer by means of the LB method. The far field characterizations revealed the success of the SWCNTs deposition demonstrating the partial filling of the nanotubes within MOFs. Also, the obtained results demonstrated that the main effect of SWCNTs filling is the significant modification of the guiding properties and thus of the local PBG at the termination of the MOF. Also, by using the LB deposition method, we demonstrate how by acting on the process parameters and especially on monolayers number and pressure conditioning at the free termination, it would be possible to optimize and tailor the SWCNTs filling enabling the local control of the MOF PBG. The proper modification of the MOF PBG features, by filling (also selectively) the MOF holes with SWCNTs, can supply, in fact, to the final device advanced functionalities and can be properly exploited to develop high performances sensors based on PBG modification as well as multimaterial and multifunctional fibers. On the basis of the retrieved results, a novel opto-chemical sensors for VOCs detection has been developed and its sensing capability has been proved by exposure to VOCs traces in a proper test chamber. The presented experimental results demonstrated that the fabrication parameters affect strongly the sensors performances and that the proposed optochemical sensor is able to perform VOCs detection with a good sensitivity and fast response times.

8. References

Abouraddy A. F., Bayindir M., Benoit G., Hart S. D., Kuriki K., Orf N., Shapira O., Sorin F., Temelkuran B., Fink Y. (2007). Towards multimaterial multifunctional fibres that see, hear, sense and communicate. *Nature*, 6, 336-347

Benabid F., Couny F., Knight J. C., Birks T. A., Russel P. St J. (2005). Compact, stable and efficient all-fibre gas cells using hollow-core photonic crystal fibres. *Nature,* 434, 488-491.

Consales M., Campopiano S., Cutolo A., Penza M., Aversa P., Cassano G., Giordano M., Cusano A., (2006) .Carbon nanotubes thin films fiber optic and acoustic VOCs sensors: performances analysis. *Sensors and Actuators B*, 118 232–242.

Consales M., (2007). Carbon Nanotubes Coated Acoustic and Optical VOCs Sensors: Towards the Tailoring of the Sensing Performances. *IEEE Transactions on Nanotechnology*, 6, 601-612.

Cusano A., Pisco M., Consales M., Cutolo A., Giordano M., Penza M., Aversa P., Capodieci L., Campopiano S. (2006). Novel Opto-Chemical Sensors Based On Hollow Fibers And Single Walled Carbon Nanotubes. *IEEE Photonics Tech. Lett.*, 18, 22, 2431 - 2433

Domachuk P., Nguyen H. C., Eggleton B. J., Straub M., Gu M. (2004). Microfluidic tunable photonic band-gap device. *Applied Physics Letters*, 84, 11, 1838-1840

Dresselhaus M. S., Dresselhaus G., Avouris P. (2001). Carbon Nanotubes: Synthesis, Structure, Properties, and Applications. Topics in Applied Physics, 80, Springer, Berlin, ISBN: 978-3-540-41086-7

Huang Y., Xu Y., Yariv A. (2004). Fabrication of functional microstructured optical fibers through a selective-filling technique. *Applied Physics Letters*, 85, 22, 29, 5182-5184

Knight J. C. (2003). Photonic crystal fibres. *Nature*, 424, 847-851

Larsen T. T., Bjarklev A., Hermann D. S., Broeng J. (2003). Optical devices based on liquid crystal photonic bandgap fibres. *Optics Express*, 11, 2, 2589-2596.

Matejec V., Mrázek J., Hayer M., Kašík I., Peterka P., Kaňka J., Honzátko P., Berková D. (2006). Microstructure fibers for gas detection. *Materials Sc. & Eng. C*, 26, 2-3, 317-321

Nielsen K., Noordegraaf D., Sørensen T., Bjarklev A., Hansen T. P. (2005). Selective filling of photonic crystal fibres. *J. Opt. A: Pure Appl. Opt.*, 7, 8, L13-L20

Penza M., Cassano G., Aversa P., Antolini F., Cusano A., Cutolo A., Giordano M., Nicolais L.(2004). Alcohol detection using carbon nanotubes acoustic and optical sensors. *Applied Physics Letters*, 85, 12, 2379-2381

Penza M., Cassano G., Aversa P., Cusano A., Cutolo A., Giordano M., Nicolais L. (2005). Carbon nanotube acoustic and optical sensors for volatile organic compound detection. *Nanotechnology*, 16, 2536-2547.

Pisco M. (2007). Optoelectronic Devices based on 1-D and 2-D Photonic Bandgap Structures for Sensing and Communication Applications. PhD Thesis

Pisco M., Consales M., Cutolo A., Penza M., Aversa P., Cusano A. (2008). Hollow Fibers Integrated with Single Walled Carbon Nanotubes: Bandgap Modification and Chemical Sensing Capability. *Sensors and Actuator B: Chemical*, 129, 1, 163-170

Pisco M., Consales M., Penza M., Aversa P., Giordano M., Cutolo A., Cusano A. (2009). Photonic Bandgap Modification in Hollow Optical Fibers Integrated with Single Walled Carbon Nanotubes. *Microwave and Optical Technology Letters*, 51, 11, 2729-2732

Zhmud B. V., Tiberg F., Hallstensson K. (2000). Dynamics of Capillary Rise. *J. Colloid Interface Sci.*, 228, 263-269

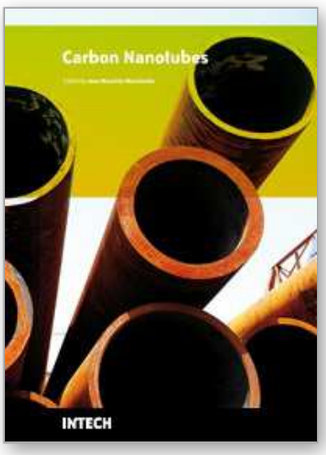

Carbon Nanotubes

Edited by Jose Mauricio Marulanda

ISBN 978-953-307-054-4
Hard cover, 766 pages
Publisher InTech
Published online 01, March, 2010
Published in print edition March, 2010

This book has been outlined as follows: A review on the literature and increasing research interests in the field of carbon nanotubes. Fabrication techniques followed by an analysis on the physical properties of carbon nanotubes. The device physics of implemented carbon nanotubes applications along with proposed models in an effort to describe their behavior in circuits and interconnects. And ultimately, the book pursues a significant amount of work in applications of carbon nanotubes in sensors, nanoparticles and nanostructures, and biotechnology. Readers of this book should have a strong background on physical electronics and semiconductor device physics. Philanthropists and readers with strong background in quantum transport physics and semiconductors materials could definitely benefit from the results presented in the chapters of this book. Especially, those with research interests in the areas of nanoparticles and nanotechnology.

INTECH
open science | open minds

InTech Europe
University Campus STeP Ri
Slavka Krautzeka 83/A
51000 Rijeka, Croatia
Phone: +385 (51) 770 447
Fax: +385 (51) 686 166
www.intechopen.com

InTech China
Unit 405, Office Block, Hotel Equatorial Shanghai
No.65, Yan An Road (West), Shanghai, 200040, China
中国上海市延安西路65号上海国际贵都大饭店办公楼405单元
Phone: +86-21-62489820
Fax: +86-21-62489821

IntechOpen